Deglaciation-enhanced mantle CO_2 fluxes at Yellowstone imply positive climate feedback

Fiona Clerc[1*], Mark D. Behn[2], and Brent M. Minchew[3]

1. MIT-WHOI Joint Program in Oceanography/Applied Ocean Science & Engineering

2. Dept. of Earth and Environmental Sciences, Boston College

3. Dept. of Earth, Atmospheric and Planetary Sciences, Massachusetts Institute of Technology

*corresponding author: fclerc@mit.edu

Non-peer reviewed pre-print submitted to *EarthArXiv*. Under review at *Nature Communications*.

Abstract

The generation of mantle melts in response to decompression by glacial unloading has been linked to enhanced volcanic activity and volatile release in Iceland[1] and in global eruptive records[2,3]. However, it is unclear whether this process is also important in magmatically-active systems that do not show evidence of enhanced eruption rates. For example, the deglaciation of the Yellowstone ice cap did not observably enhance volcanism[4], yet Yellowstone may still have released large volumes of CO_2 to the surface due to the crystallization of melts at depth. Here we develop models to simulate mantle melt production and volatile release associated with the deglaciation of Yellowstone and Iceland. In agreement with previous work[1], we find mantle melt production in Iceland is enhanced 33-fold during deglaciation, generating an additional 3728 km^3 of melt and releasing an additional 31–51 Gt of CO_2. Beneath Yellowstone, we find mantle melt production is comparably enhanced 19-fold during deglaciation, generating an additional 815 km^3 of melt, though thicker lithosphere may prevent the transport of this melt to the surface. These melts segregate an additional 135–230 Gt of CO_2 from the mantle, representing a ~23–39% increase of the global volcanic CO_2 flux (if degassed during deglaciation). Our results suggest deglaciation-enhanced mantle melting is important in continental settings with partially molten mantle (potentially Greenland and West Antarctica) and may result in positive feedbacks between deglaciation and climate warming.

Main

As an ice mass retreats and unloads the Earth's surface, the underlying mantle rebounds and undergoes a reduction in pressure. If the mantle is above the solidus, this decompression generates additional melting relative to any background rate. Enhanced mantle melting can result in increased volcanic activity[1,5], which in turn may incite the release of aerosols into the atmosphere, the acceleration of glacier flow by geothermal heating, and outburst flooding from glacial lakes. The rapid flow of the Northeast Greenland Ice Stream has been attributed to elevated geothermal heat fluxes (GHF) due to volcanism[6] or the passage of the Iceland plume, perhaps influencing the mass of the Greenland Ice Sheet over glacial-interglacial cycles[7]. Beneath the West Antarctica Ice Sheet (WAIS), ice flow could be enhanced by elevated GHF from subglacial volcanism[8,9] or a mantle plume[10]. Understanding whether deglaciation enhances continental and/or hotspot magmatism has implications for the retreat of the Greenland and West Antarctic Ice Sheets.

Increased mantle melting also enhances the extraction of CO_2 from the mantle. If released to the surface, the additional magmatic CO_2 can impact the Earth's climate. During the last deglaciation, subaerial volcanoes are thought to have erupted up to 1000–5000 Gt of additional CO_2 (refs. [2,3]). Changes in sea-level associated with glacial-interglacial cycles may also enhance CO_2 emissions from mid-ocean ridge volcanoes[11]. However, little work has focused on the enhancement of diffuse subaerial CO_2 emissions from hydrothermal systems and dormant volcanoes, despite their large present-day CO_2 flux of 170 Mt/yr, representing roughly half of the modern global volcanic CO_2 flux[12].

The link between deglaciation and enhanced mantle melting is most strongly established in Iceland[1,5,13], where increases in eruptive volumes coincide with the most rapid stage of the Late Weischelian deglaciation of the Iceland ice sheet from 11–10 ka (BP). While shallower crustal processes may also modulate the magmatic response to deglaciation, the importance of enhanced mantle melting is evidenced by the magnitude of deglacial eruptive rates and the coeval depletion of incompatible trace elements, first modelled by Jull and McKenzie[1] (hereafter JM96).

By comparison, deglaciation-enhanced melting in continental mantle has not been quantified (with the exception of global ice mass loss scalings[2]), and observations of enhanced volcanism during deglaciation in intraplate settings are primarily attributed to the triggering of crustal magma chambers[14,15]. For example, Yellowstone is magmatically active and has experienced rapid deglaciation. During the Pinedale (22–13 ka) and Bull Lake (140–150 ka) glaciations, ice caps covered the Yellowstone caldera and beyond, extending 100 km in radius[4]. While the Pinedale deglaciation occurred during a period of volcanic quiescence, the Bull Lake deglaciation occurred during the most recent eruptive episode in Yellowstone, the Central Plateau Member rhyolites (170–70 ka). Geological evidence suggests many of these eruptions are syn-glacial[16,17]. The Central Plateau Member rhyolites were erupted from a large upper crustal sill, maintained by an extensive deeper magmatic system potentially fed by a mantle plume[18]. During the deglaciation interval there is no evidence that eruptive rates were heightened, nor that the magmatic system was otherwise altered, relative to background rates/trends. However, Yellowstone's present-day magmatic CO_2 flux (~5% of the modern global flux[19]) is released not by eruptions, but by the crystallization of magmas at depth[19]. Thus, it remains unclear whether mantle melting rates and associated volatile fluxes are significantly enhanced under thicker continental lithosphere, particularly as glacially induced pressures are attenuated with depth[1], and by extension whether the singularly strong response of Iceland is related to the unique juxtaposition of the Icelandic mantle plume and the Mid-Atlantic ridge.

In this study, we model deglaciation-enhanced mantle melting in both Iceland and Yellowstone, to gain insight into local eruption rates and the potential for enhanced CO_2 fluxes from each system. We use the mantle convection code ASPECT[20,21] to simulate changes in pressure and melt production due to glacial unloading for Iceland and Yellowstone (see Methods). The 2-D models are first run to steady-state to resemble present-day “background” behavior (Figure 1) and are then loaded/unloaded using the reconstructed ice load for each system. The models are unloaded by decreasing the ice sheet radius at a constant rate over a prescribed deglaciation interval (1000 years for Iceland, 2000 years for Yellowstone), simulating the retreat of the ice margin. The mantle melt production rate is the rate of melt fraction change integrated spatially. We also calculate trace element concentrations and estimate the flux of CO_2 segregated from the mantle by melts and the flux of CO_2 exsolved to the surface. Finally, we estimate the heat released by the emplacement of additional melts.

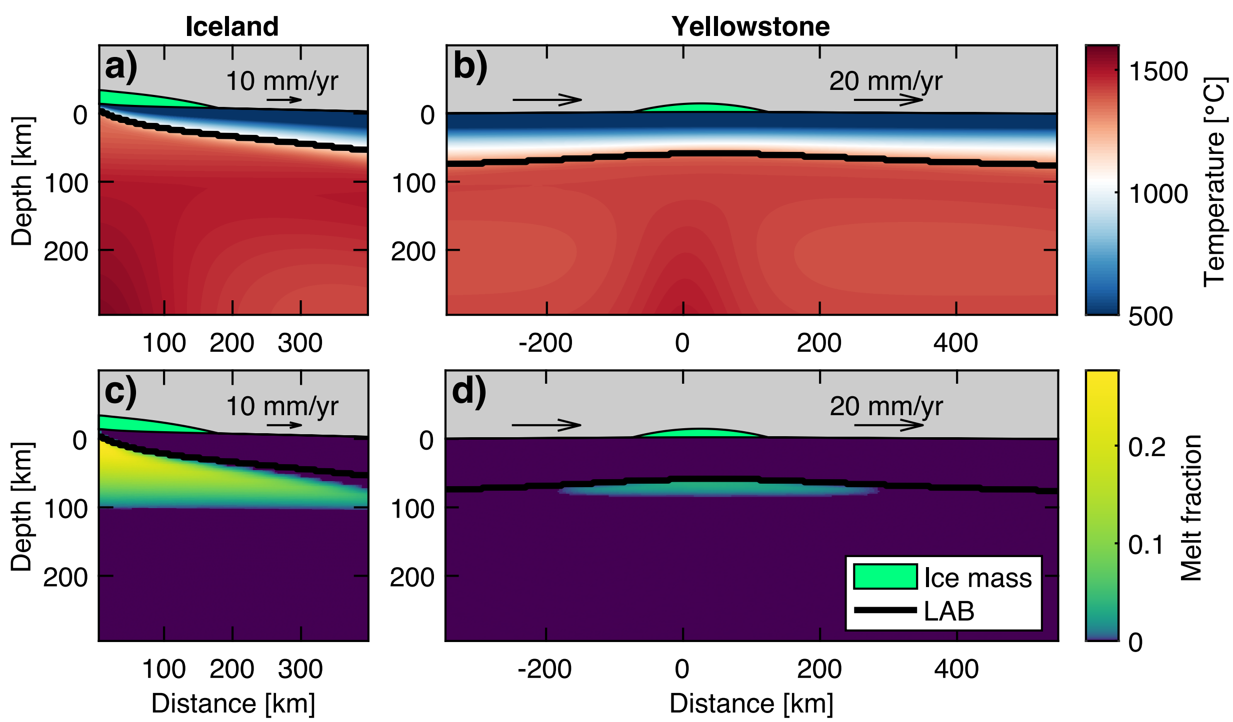

Figure 1. Background mantle temperatures and melt fractions, prior to unloading.

Temperatures beneath a) Iceland and b) Yellowstone are plotted in red-blue. The thick black line *is the lithosphere-asthenosphere boundary (LAB). The green parabola represents the ice volume at its maximum (10-fold vertical exaggeration). Black arrows indicate imposed plate motions. Melt fractions in blue-green plotted for c) Iceland and d) Yellowstone.*

Deglaciation melting in Iceland

We first model mantle melt production rates underneath Iceland (Figure 2; "primary run") and additionally benchmark our approach against JM96 (Supplemental Information). Prior to unloading, the mantle flow field is a combination of passive corner flow from plate spreading and dynamic flow from the thermally buoyant plume (red arrows in Figure 2a). The integrated background melting rate over the entire domain is 0.115 km^3/yr (orange line in Figure 3b; see Methods).

As the mass of the ice sheet is unloaded, the underlying mantle rebounds (Figure 2c, red arrows), inducing large rates of decompression (Figure 2c, teal). The background flow is still present but is overshadowed by the much greater (>0.3 m/yr) glacial isostatic adjustment. Due to the thin lithosphere, the mantle response is localized, roughly confined within the margin of the retreating ice sheet. The large rates of decompression greatly enhance melt production rates (Figure 2d) throughout the ridge melting triangle. When spatially integrated throughout the entire domain, the melt production rate increases by an "enhancement factor" of ~33 during the deglaciation interval, producing 0.43 km^3/yr of melt (Figure 3b, black line). JM96 predict similar increases in melt production during deglaciation using slightly different model assumptions (see Supplementary Information).

Overall, we find that the rates of enhanced melt production depend primarily on the thermal structure and background melt fractions prior to deglaciation, and the total rate and volume of ice removed. We test different styles of ice sheet retreat (Figure S4), but find that the total melt production by the end of deglaciation scales most closely with the total change in ice sheet volume. Under larger spreading rates or mantle temperatures, melt fractions increase and the zone of enhanced melting broadens in horizontal extent. Yet the relative enhancement in melting is smaller under these more productive conditions (Figure S5).

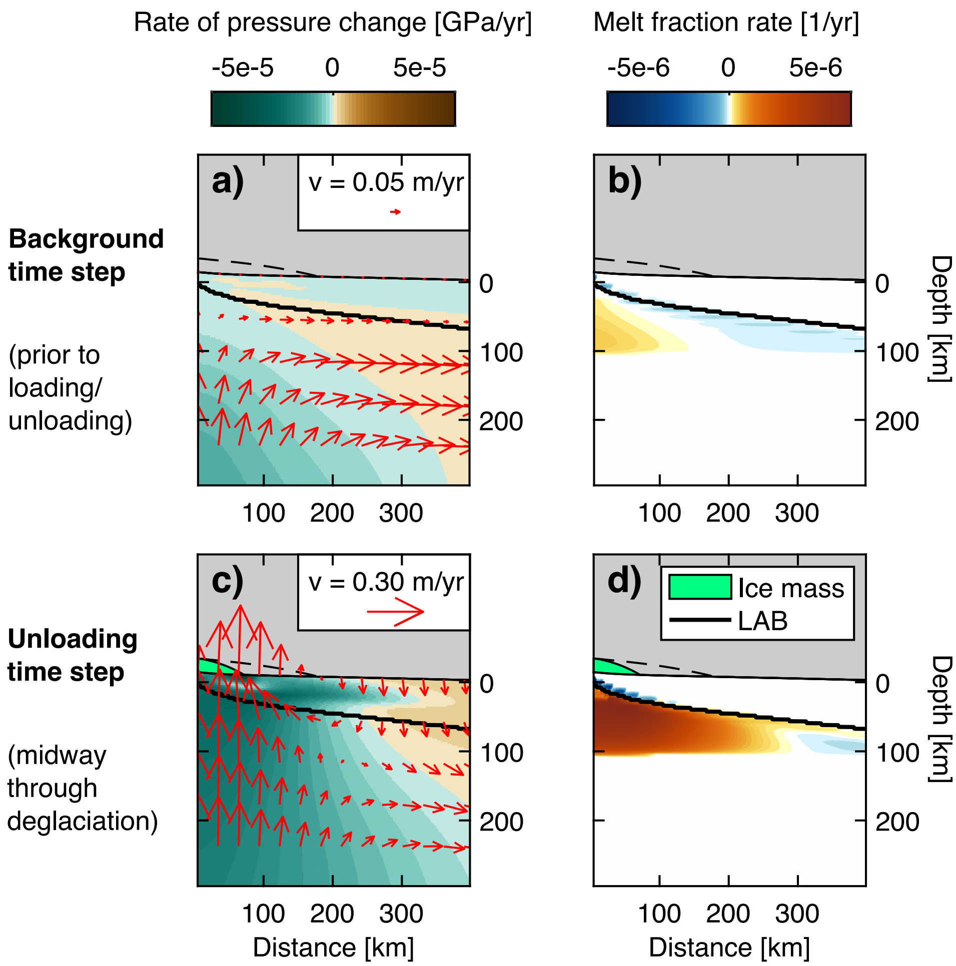

Figure 2. Modeled melt production due to deglaciation of Iceland ice sheet. *The ice sheet is represented by the green parabola at a given time step and by the dashed black line at its maximum extent. Rates of pressure change are colored teal-brown (a,c) and rates of melt fraction change are colored blue-orange (b,d). Top row shows a model time step prior to any*

glacial loading/unloading, while bottom row shows a time step 500 years following deglaciation onset. Red arrows show mantle flow; the thick black line is the LAB (T = 1100 ℃).

We estimate the concentration of CO_2 in the melt and the flux of CO_2 released to the surface. We calculate the partitioning of CO_2 into the melt using the retained melt fraction formulation[22], which can reproduce the magnitude of the observed[5,23] depletion in trace element concentrations due to deglaciation (see Methods and Figure S9a). Our background CO_2 fluxes (orange lines in Figure 3d) are within the range inferred from helium fluxes[24]. During the deglaciation, we calculate that for a mantle CO_2 content of 300–500 ppm (see Methods), an additional 31–51 Gt of CO_2 is released over 1 kyr (dash-dotted black line, Figure 3d), corresponding to a 13-fold increase over the background flux. This additional CO_2 is likely not released instantaneously, but is slowed by processes such as melt migration[25]. This value is of the same order of magnitude as prior estimates[25], which found an extra ~165 Gt CO_2 was released over the 11 kyrs following deglaciation for a mantle CO_2 content of 285 ppm.

Finally, we examine the conditions under which the heat released by the emplacement of the additional melts may reach the surface. The emplacement of our steady-state melt production rate at a depth of 10 km releases 8.7 GW of heat (comparable to the 8 GW estimated in a similar calculation[26]). This flux may be transferred conductively to the surface over long time scales, and is consistent with borehole measurements from outside the rift zone[26]. During the deglaciation, we estimate the emplacement of the additional melts releases 281 GW at depth, for a total of 9×10^{21} J over the entire interval. For comparison, the energy required to melt a 100,000 km^3 Icelandic ice sheet near its melting point is 30×10^{21} J.

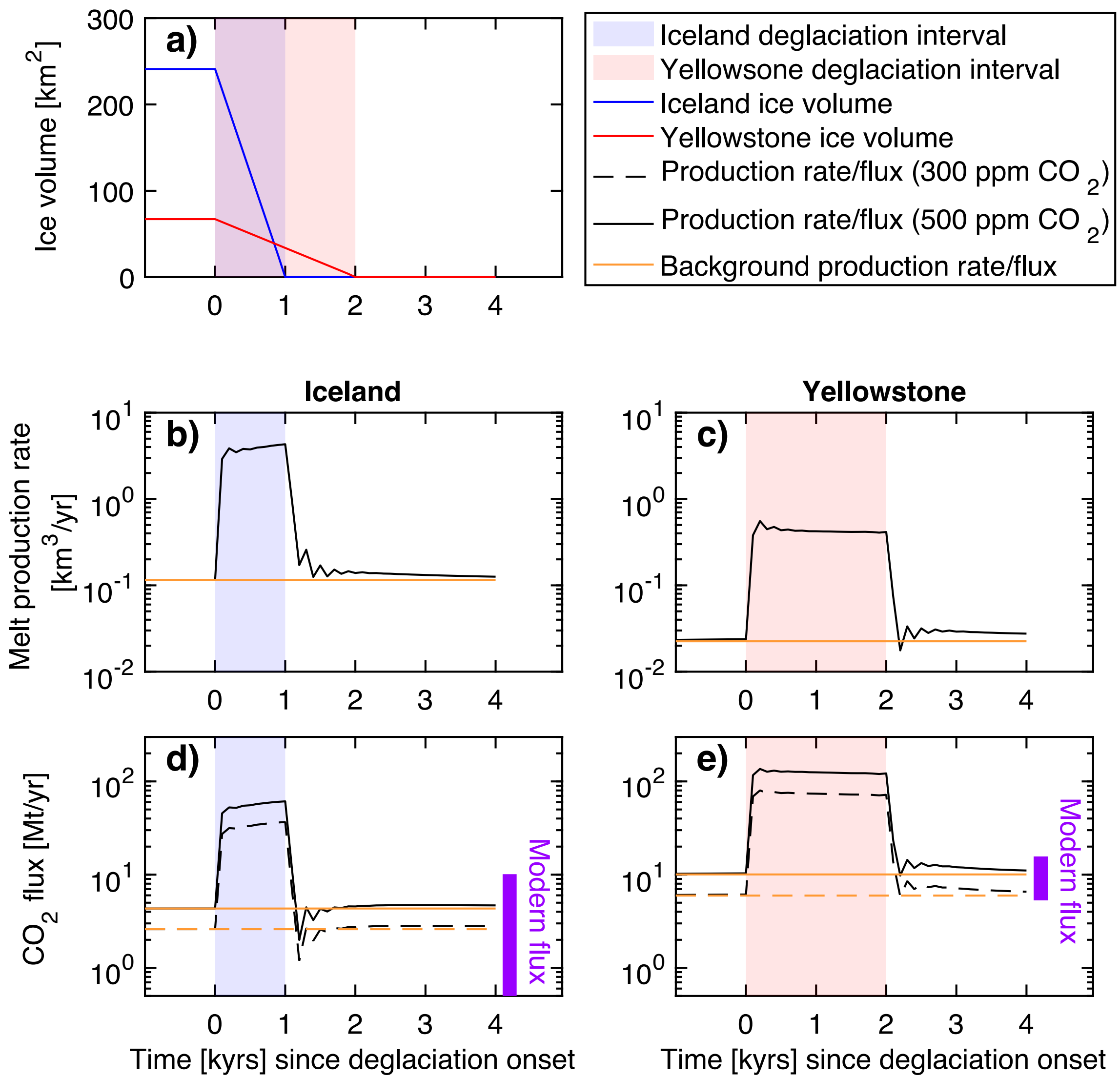

Figure 3. Evolution of melt production rate and CO_2 flux during deglaciation. *(a) Ice volumes used as model forcings for Iceland (blue) and Yellowstone (red) during the deglaciation intervals (shaded). Melt production rates (black lines) for (b) Iceland and (c) Yellowstone; background rates from time steps prior to loading/unloading are plotted in orange. CO_2 fluxes for (d) Iceland and (e) Yellowstone assuming mantle source CO_2 concentrations of 300 and 500 ppm are plotted as dashed and solid lines, respectively. Estimates of modern magmatic CO_2 fluxes for Iceland*[24] *and Yellowstone*[19] *are denoted by purple bars.*

Deglaciation melting in Yellowstone

We next estimate how deglaciation affects mantle melt production rates associated with the Yellowstone plume. Prior to unloading, the background mantle flow field represents a combination of shearing from the westward motion of the North American plate and uplift from the plume (Figure 4a, red arrows). Melts are produced over the depth interval from 90 to 70 km, over a 300-km wide region (orange colors in Figure 4b). The background mantle melt production rate of 0.022 km^3/yr represents the rate of emplacement of basalts, assuming efficient melt extraction.

During the deglaciation, we find that the enhancement of melting beneath Yellowstone is comparable to Iceland (Figure 3b,c), in spite of the thickness of the continental lithosphere and the smaller rates of unloading from the Yellowstone ice cap. The upper asthenosphere upwells at a rate of 0.1 m/yr due to a combination of the background plume/plate flow and isostatic adjustment (Figure 4c). The zone of positive melt production grows laterally and extends to shallower depths of 60 km (Figure 4d). The total melt production rate increases to 0.43 km^3/yr during deglaciation, representing a 19-fold enhancement of melting and an additional 815 km^3 of melt over the entire deglaciation (Figure 3c). Modelled trace element profiles predict a ~30% depletion in light rare Earth elements (LREE) during unloading, relative to background compositions (Figure S9b).

We also test the response of a transient upper mantle thermal anomaly without a plume tail (Figure S5) and higher melt production rates (Figure S6). In the case lacking a plume tail, unloading of the transient upper mantle thermal anomaly yields melt production rates that are almost as high (93%) as the case with a plume tail (Figure S7). In cases with higher melt production rates, greater volumes of additional melt are generated during deglaciation (see Methods).

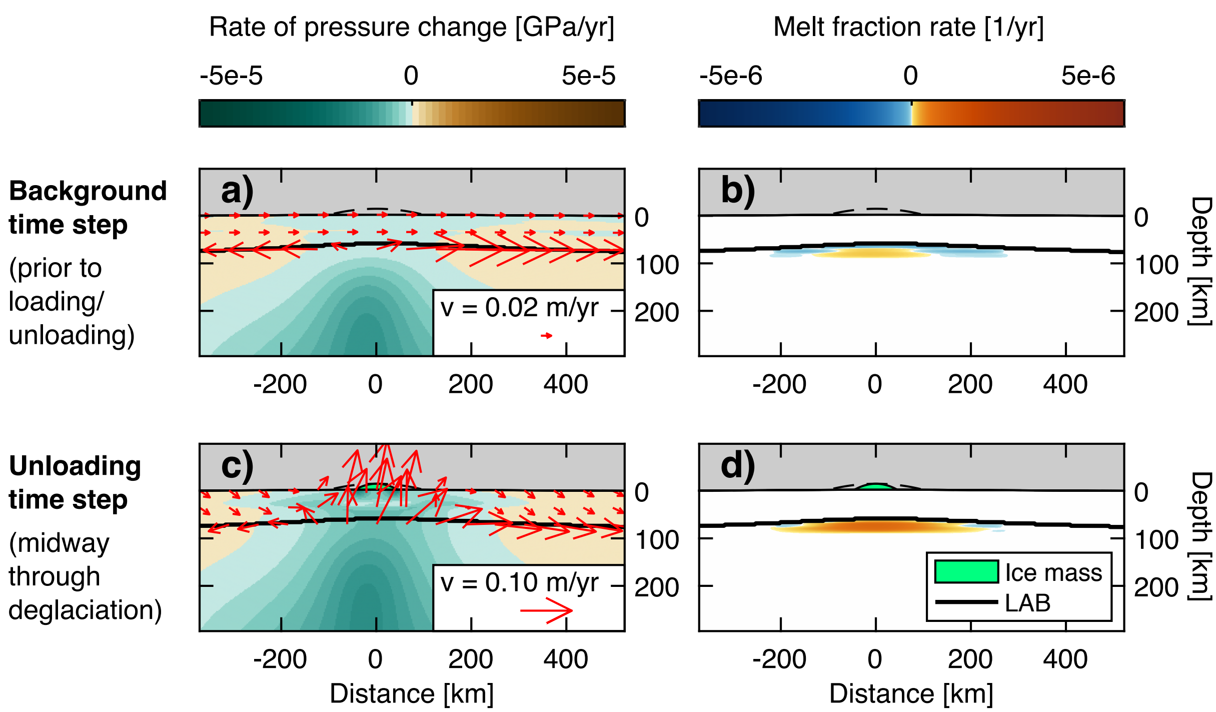

Figure 4. Modeled melt production due to deglaciation of Yellowstone ice cap*. The ice cap is represented by the green parabola at a given time step and by the dashed black line at its maximum extent. Rates of pressure change are colored teal-brown (a,c) and rates of melt fraction change are colored blue-orange (b,d). The top row shows a model time step prior to any glacial loading/unloading, while the bottom row shows a time step 1000 years following deglaciation onset. Red arrows show mantle flow, the thick black line is the LAB (T = 1300℃).*

The enhancement in melt production implies more carbon is extracted from the mantle and released to the surface as CO_2. Extrapolated surface measurements of diffuse outgassing at Yellowstone[19] predict a modern-day CO_2 flux of 11–22 Mt/yr. Carbon and helium isotopes suggest that ~50–70% of this flux may be attributed to mantle magmatism[19]. Assuming mantle

CO_2 concentrations of 300–500 ppm (within the range observed in mantle xenoliths[27]), we obtain background mantle-derived CO_2 fluxes of 6.0–10.1 Mt/yr, in agreement with the above constraints. During unloading, the CO_2 flux increases to 74–125 Mt/yr, representing a 12-fold enhancement if released during the deglaciation. Over the entire deglaciation, we estimate the release of an additional 135–230 Gt CO_2 to the surface.

The large enhancement in melting may transfer additional heat from the mantle to the crust or surface. Melts derived from the mantle are thought to recharge a large upper crustal sill, imaged seismically at depths of 4–14 km (ref. [18]). We estimate the emplacement of the 0.022 km^3/yr background melt production rate at a depth of 14 km releases 3.8 GW of heat, comparable to the 4–8 GW extrapolated from chloride fluxes[28]. During deglaciation, the emplacement of the additional melts would impart an additional 69 GW of heat at depth, for a total of 4×10^{21} J over the deglaciation interval. The energy required to melt a 20,000 km^3 Yellowstone ice cap near its melting point is 6×10^{21} J.

Deglaciation melting in continental settings

Our calculations imply that Yellowstone underwent a similar enhancement in melting due to deglaciation as did Iceland. While the surface and geochemical expressions of this enhanced melting are observed in Iceland, none of the basaltic flows in Yellowstone have been precisely dated to either deglaciation[29,30]. Moreover, even if deglacial basaltic flows are buried beneath newer material, modelled trace element depletions are within the range of existing observations, implying deglaciation signatures may not be resolvable (Figure S9b). We infer that processes governing melt migration through the lithosphere and crust mitigate volcanic activity despite enhanced melting beneath Yellowstone. Understanding the transfer of the mantle melts to the surface is further complicated by the influence of unloading on the shallower magmatic system. Various studies have examined how magma chambers can be triggered by deglaciation[14,15]. Mantle melts may be pumped upwards as the continental lithosphere flexes during deglaciation[31]. We suspect that relative to Iceland, the thickness of the lithosphere beneath Yellowstone and the complexity of its magmatic system make it more difficult to efficiently transport mantle melts to the surface.

Even in the absence of anomalous eruption rates, large enhancements in mantle melting beneath Yellowstone can influence the crustal magmatic system. Bimodal basalt-rhyolite volcanism in Yellowstone may be explained by the co-existence of a rhyolitic upper crustal sill and a deeper basaltic reservoir[18]. The emplacement of mantle-derived melts into or near the upper crustal sill fuels rhyolitic eruptions, representing a source of heat and mass[32]. During the deglaciation we calculate an additional 815 km^3 of mantle melt, ~16% of the 5000 km^3 of silicic melt estimated to be in the upper crustal sill today[18]. Similarly, the additional 4×10^{21} J of heat we calculate could be imparted to the sill during the deglaciation, sufficient to melt an additional 5800 km^3 of near-solidus silicic melts, more than doubling the upper crustal sill volume. These upper-bound estimates illustrate that the emplacement of a large fraction of deglacial melts into or near the upper crustal sill may influence its dynamics or composition. Alternatively, the effect on the shallow magmatic system may be imperceptible, if for example the mantle melts travel slowly through the mantle and crust or are emplaced far from the sill.

The flux of CO_2 released to the surface by the crystallization of mantle melts at depth is less sensitive to upper crustal processes and may be the most consequential impact of deglaciation-enhanced melting beneath Yellowstone. The release of an additional 135–230 Gt of CO_2 is likely not instantaneous (as might be implied by Figure 3e). Instead, CO_2 ascension will be slowed by magmatic and/or hydrothermal processes. For example, if the additional CO_2 from Yellowstone is degassed slowly over 20 kyr (implying melts travel through the lithosphere and lower crust at a rate of 2 m/yr), the enhanced flux would represent a ~2–4% increase in the global volcanic CO_2 flux[12]. In this scenario, the present-day Yellowstone flux may still be elevated by ~7–12 Mt/yr due to enhanced melting during the Pinedale deglaciation. Alternatively, if the enhanced CO_2 flux is degassed rapidly during a 2-kyr deglaciation, the enhanced flux would represent a ~21–39% increase in the global volcanic CO_2 flux[12] and could be accompanied by deglaciation-enhanced fluxes from other volcanoes, such as arcs[2,3]. The additional CO_2 from Yellowstone would increase the global deglacial CO_2 flux from active subaerial volcanoes since the last glacial maximum[2] by 3–23%. For perspective, it has been proposed that the global deglacial CO_2 flux from arc volcanos was responsible for the 40 ppm increase in atmospheric CO_2 between 13–7 ka (ref. [2]). It is therefore possible that the enhanced release of magmatic CO_2 from Yellowstone also plays an important role in this positive feedback between deglaciation and climate.

Another way in which deglaciation, climate warming, and volcanism may be linked is by the acceleration of ice flow due to volcanically enhanced geothermal heat fluxes (GHF). If heat associated with the emplacements of melt at depth was transported to the surface, it would be sufficient to melt 67% of the Yellowstone ice cap and 30% of the Iceland ice sheet. Large GHFs would maintain a thawed, water-saturated basal till and would soften overlying ice, dynamically enhancing the mass loss of ice[33]. Yet in order to influence ice flow in Yellowstone, this additional heat must travel >10 km through the crust and reach the surface within the deglaciation interval (~1 kyr). The thermal conduction of heat from intruded basalts is negligible at ~kyr timescales[34]. Instead, advective heat transfer would require mass fluxes of magmatic and hydrothermal fluids of >10 m/yr in order to affect ice dynamics during the deglaciation interval. The modelled response of the Iceland ice sheet to GHFs enhanced 50% from present-day values is minimal[35]. Yet given the colocation of paleo ice streams and geothermal features in Iceland[36], the effect of a larger (as estimated here) and more localized GHF enhancement remains an important topic to be explored. Beneath Yellowstone, rising melts may induce a response in the hydrothermal system by imparting heat[37] or CO_2 (ref. [38]). In fact, larger hydrothermal explosion craters are observed during the last glaciation, although this effect was attributed to changes in the water table due to lake drainage[39]. The reactivation of faults due to deglaciation[40] conceivably also influences hydrothermal fluid flow.

Implications for West Antarctica and Greenland

Placing our findings in a broader context, we suggest magmatically-active continental systems may experience enhanced mantle melting in response to deglaciation. Moreover, deglaciation may enhance transient melting anomalies that would not be otherwise productive, supporting the idea that, if present, remnant melts beneath Greenland may be influenced by deglaciation[7]. The transient melting anomaly model (Figure S7) implies deglaciation can enhance melting in the upper mantle over a range of geodynamic conditions, in settings characterized by a partially molten mantle.

In particular, West Antarctica is volcanically active[41] and characterized by relatively thin (60–110 km) lithosphere[42]. Other tectonic similarities between the West Antarctic Rift System (WARS) and Yellowstone include the possible existence of a mantle plume[43] and extensional lithospheric stresses. During some interglacials, paleo proxies suggest the collapse of the West Antarctica Ice Sheet (WAIS) (ref. [44]) and models predict the loss of millions of km^3 of ice over short (~kyr) timescales[45]. The horizontal extent of the WAIS also implies deglacial unloading will generate larger rates of decompression at asthenospheric depths compared to our calculations for Yellowstone. Finally, while the total flux of CO_2 from West Antarctic volcanism is unconstrained, other continental rift systems are important CO_2 emitters[12] and the WARS mantle is rich in CO_2 (ref. [46]). Thus, melt production rates and associated CO_2 fluxes released into the atmosphere may be greatly enhanced under WAIS collapse and could drive a positive feedback with climate warming. As modern elevated GHF already influence ice flow[8–10], deglacially enhanced melting may further impart heat to the base of the WAIS and accelerate its collapse. Understanding the magnitude of deglacially enhanced melting beneath West Antarctica has implications for global carbon budgets, climate, and the evolution of the WAIS over millennial time scales.

---

4. Methods

We examine deglaciation-enhanced mantle melting beneath Iceland and Yellowstone using the mantle convection code ASPECT[20,21]. The models are sufficiently idealized to facilitate comparison between both settings, yet capture key geodynamic differences and match various observations. We estimate CO_2 and heat fluxes to understand the surface impact.

The mantle is assumed to behave as a Newtonian visco-elasto-plastic material with a temperature-dependent viscosity. Viscosities are calculated for dry dislocation creep[47] and converted to a Newtonian form yielding asthenospheric viscosities of $0.5 – 1.0 \times 10^{19}$ Pa s in the absence of a plume thermal anomaly. Elasticity is characterized by a shear modulus of 10^{10} Pa. A

Mohr-Coulomb failure law allows rapid deformation at the Iceland ridge axis during spin-up, otherwise plasticity is not activated.

Mantle potential temperatures of 1300°C for Iceland and 1320°C for Yellowstone are assumed in the absence of a plume. Plumes are initiated with a thermal Gaussian anomaly at 600 km depth, centered at x = 0 km (Figure 1). The plumes' excess temperature and radius at 600-km depths are 175°C and 100 km for Iceland and 80°C and 70 km for Yellowstone, respectively, in accordance with previous work benchmarked against geophysical observations[48–50]. The plume underneath Iceland is centered beneath a symmetrical ridge axis, while the Yellowstone plume is located in the middle of an asymmetrical domain. During model spin-up, the top boundary condition is driven by plate motions (10 mm/yr for Iceland, 20 mm/yr for Yellowstone). The remaining boundaries are open, with the exception of the free-slip symmetry condition at the Iceland ridge axis. Domain widths are 1200 km for Iceland and 2700 km for Yellowstone. The models are run until the thermal structure and flow field stabilize (10–30 Myr).

The flow through the open boundaries is then fixed to the steady-state value, and the top boundary becomes a free surface that deforms in response to applied pressures. After the glacial load is applied, the model is again allowed to stabilize to rule out the influence of the glaciation. The Iceland ice sheet is simulated as a parabola 180 km in radius and 2 km high (as in JM96). However, we assume the load retreats vertically from the margins, while JM96 kept the load radius constant and horizontally thinned the ice sheet thickness. We compare the horizontally thinned load from JM96 (constant radius, decreasing thickness), the vertically retreating load (decreasing radius, constant maximum thickness) shown in Figure 2, and a horizontally and vertically retreating smaller load (following refs. [35,51]). In vertically retreating simulations, the melt production rate increases through time as the zone of maximum decompression migrates towards the ridge axis where the load is centered (Figure S4). For the Yellowstone ice cap, we use a radius of 100 km and a height of 1.25 km, yielding a volume of 20,000 km^3 (ref. [4]). Unloading the ice cap horizontally instead of vertically does not influence melt production rates (Figure S8a). The dimensions of the Yellowstone ice cap correspond to the most recent and well-constrained Pinedale deglaciation (15–14 ka), we assume the more relevant penultimate Bull Lake glaciation (~150 ka) retreated similarly. Lengthening the duration of the deglaciation reduces the melt production rate; however, the total volume of melt produced over the entire deglaciation is unchanged and depends solely on the volume of ice lost (Figure S8b).

The rate of melt fraction change depends on the material derivative of the pressure field, which includes both instantaneous (elastic) changes in pressure and isostatic rebound. We also include the dependence of the melt fraction rate on the temperature field due to the effects of latent heat (as in ref. [52]). We use a dry peridotite solidus[53], implying our models underestimate melt volumes under hydrated mantle conditions. Melt fractions (Figure 1c,d) and their dependence on pressure/temperature remain relatively constant through time as the deglaciation time scales are short.

The Iceland melt production rate is approximately scaled to 3-D using a length scale of 100 km (half the plume head width[48]), although comparisons to the JM96 benchmark are presented in 2-D. The background melt production rate of 0.115 km^3/yr for Iceland is equivalent to a steady-state crustal thickness 128 km for a 10 mm/yr spreading rate and mantle and crustal densities of 3000 and 2700 kg/m^3, respectively. This is higher than the observed crustal thickness of 20–40 km (ref [54]); but consistent with prior modeling studies that argue the excess crustal material is redistributed laterally along axis[48]. Thus our 2-D slice through the plume center represents the maximum melt production and the total 3-D rate would average with less productive regions away from the plume center. We ran the same model without the plume and obtain a crustal thickness of 7 km, typical of slow-spreading mid-ocean ridges[55].

The 3-D melt production rate for Yellowstone is calculated by radial integration of melt fraction rates. The maximum melt fraction is 3.5% and the mantle potential temperature (including the excess plume temperature) is 1400°C, consistent with geophysical and geochemical constraints[56,57]. The absence of melts at depths >90 km in our model is attributable to the use of a dry solidus. The melts must leave the asthenosphere rapidly to avoid refreezing in the outer melt region, which reaches depths of 60 km at the shallowest point (Figure 4b; blue colors). The background melt production rate of 0.022 km^3/yr is comparable to the estimated emplacement rate of basalts into the crust (0.005–0.025 km^3/yr) based on uplift rates and thermal arguments[19,29]. The simulation in which the plume tail is removed has a smaller background melt production rate of 0.006 km^3/yr, due to the absence of uplift from the lower mantle. Following alternative estimates derived from chloride[58] and CO_2 flux[59] considerations, we also vary the mantle temperature (including the excess plume temperature) to 1420°C and 1460°C and obtain melt production rates of 0.05 and 0.3 km^3/yr, respectively (Figure S6). The simulation with the 1420°C mantle temperature produces an extra 1448 km^3 of melt (representing a 13-fold enhancement) and 99–169 Gt of CO_2. The simulation with the 1440°C mantle temperature produces an extra 3068 km^3 of melt (representing a 5-fold enhancement) and 29–54 Gt of CO_2. Under more productive conditions, the extra CO_2 released is smaller as we must assume lower source mantle CO_2 concentrations to match modern CO_2 fluxes (Figure S6b).

In both Iceland and Yellowstone, we calculate trace element concentrations using a non-modal retained batch melting formulation[22], assuming partition coefficients for peridotite melting[60] and a retained melt fraction of 1 wt.%. The element concentrations in the pooled melts are weighted by the melt production function, and vary during unloading. During the deglaciation of Iceland, trace element concentrations provide evidence that mantle melting was enhanced, as incompatible light rare Earth elements (LREE) become more diluted under greater melting rates[1,5,23]. We compare the percent change in the LREE compositions between the unloading period and a background time step (Figure S3). While our method and partition coefficients differ from those used by JM96, we obtain similar changes before and after unloading in our benchmark case with otherwise identical assumptions and parameters (~15% change for La). In the primary run (Figure 2) the dynamically consistent thermal structure implies a wider melting region (see Supplementary Information), leading to further depletion of trace elements during unloading relative to the background (~60%), approaching the observed depletions of ~70% (Figure S9a).

Using the same approach and assuming CO_2 partitions into the melt similarly to barium[61], we estimate the flux of CO_2 segregated from the mantle by melts. If the melts are emplaced at depth, greater lithostatic pressures imply increased solubility of CO_2 in the melt. For Iceland, we assume the melts are erupted or emplaced at shallow depths such that the CO_2 is perfectly outgassed to the surface. Melt inclusion compositions[62] indicate the bulk concentration of CO_2 in the Icelandic mantle is a mix of a deep mantle component containing ~1350 ppm CO_2 and a depleted mantle component containing ~120 ppm CO_2 (ref. [63]). To simulate different mixtures of these components, we show results for source concentrations of 300 and 500 ppm CO_2 in Figure 4d. For Yellowstone, we assume the melts crystallize at 14 km, the base of the upper crustal sill[18]. This implies 0.25 wt.% CO_2 is retained in carbonate form[64], such that 80% of the CO_2 segregated from the mantle is released to the surface. We compare the flux of CO_2 exsolved to the surface with published estimates of CO_2 released into the atmosphere by magmatic activity

(Figure 3d,e). While we explore different mantle source CO_2 concentrations, we do not model the effect of these different concentrations on the degree of melting. Omission of low-degree carbonate melting does not affect melt volumes substantially, but could cause underestimates in CO_2 fluxes.

We use the melt production rates to estimate geothermal heat fluxes. We assume the basaltic mantle melts have a density of 2800 kg/m^3, specific heat of 1500 J/kg/K, and latent heat of 400 kJ/kg (ref. [65]). From our numerical model, we obtain the difference in temperature between the depths of melt generation and emplacement. For Iceland, we consider the emplacement of melts at a depth of 10 km (ref. [26]) and assume the melts are 300°C warmer than the surrounding crust. For Yellowstone, we consider the emplacement of all the melts near the base of the upper crustal sill (~14 km), and assume that the melts are 1000°C warmer than the surrounding crust. The heat released as melts cool and crystallize is scaled by the emplacement rate, yielding an estimate of the heat imparted by the melts at the depth of emplacement. We also assume silicic melts have a latent heat of 300 kJ/kg and density 2300 kg/m^3 (ref. [65]), and ice has a latent heat of 334 kJ/kg and density 900 kg/m^3.

References

1. Jull, M. & McKenzie, D. The effect of deglaciation on mantle melting beneath Iceland. *J. Geophys. Res. Solid Earth* (1996).

2. Huybers, P. & Langmuir, C. Feedback between deglaciation, volcanism, and atmospheric CO 2. *Earth Planet. Sci. Lett.* (2009). doi:10.1016/j.epsl.2009.07.014

3. Watt, S. F. L., Pyle, D. M. & Mather, T. A. The volcanic response to deglaciation:

Evidence from glaciated arcs and a reassessment of global eruption records. *Earth-Science Reviews* (2013). doi:10.1016/j.earscirev.2013.03.007

4. Licciardi, J. M. & Pierce, K. L. History and dynamics of the Greater Yellowstone Glacial System during the last two glaciations. *Quaternary Science Reviews* (2018). doi:10.1016/j.quascirev.2018.08.027

5. Maclennan, J., Jull, M., McKenzie, D., Slater, L. & Grönvold, K. The link between volcanism and deglaciation in iceland. *Geochemistry, Geophys. Geosystems* (2002). doi:10.1029/2001GC000282

6. Fahnestock, M., Abdalati, W., Joughin, I., Brozena, J. & Gogineni, P. High geothermal heat flow, basal melt, and the origin of rapid ice flow in central Greenland. *Science (80-.).* (2001). doi:10.1126/science.1065370

7. Alley, R. B. *et al.* Possible Role for Tectonics in the Evolving Stability of the Greenland Ice Sheet. *J. Geophys. Res. Earth Surf.* (2019). doi:10.1029/2018JF004714

8. Blankenship, D. D. *et al.* Active volcanism beneath the West Antarctic ice sheet and implications for ice-sheet stability. *Nature* (1993). doi:10.1038/361526a0

9. Vogel, S. W. & Tulaczyk, S. Ice-dynamical constraints on the existence and impact of subglacial volcanism on West Antarctic ice sheet stability. *Geophys. Res. Lett.* (2006). doi:10.1029/2006GL027345

10. Seroussi, H., Ivins, E. R., Wiens, D. A. & Bondzio, J. Influence of a West Antarctic mantle plume on ice sheet basal conditions. *J. Geophys. Res. Solid Earth* (2017).

doi:10.1002/2017JB014423

11. Burley, J. M. A. & Katz, R. F. Variations in mid-ocean ridge CO 2 emissions driven by glacial cycles. *Earth Planet. Sci. Lett.* **426**, 246–258 (2015).

12. Werner, C. *et al. Carbon Dioxide Emissions from Subaerial Volcanic Regions - Two Decades in Review*. *Deep Carbon - Past to Present* (2019).

13. Sinton, J., Grönvold, K. & Sæmundsson, K. Postglacial eruptive history of the Western Volcanic Zone, Iceland. *Geochemistry, Geophys. Geosystems* (2005). doi:10.1029/2005GC001021

14. Jellinek, A. M., Manga, M. & Saar, M. O. Did melting glaciers cause volcanic eruptions in eastern California? Probing the mechanics of dike formation. *J. Geophys. Res. Solid Earth* (2004). doi:10.1029/2004JB002978

15. Glazner, A. F., Manley, C. R., Marron, J. S. & Rojstaczer, S. Fire or ice: Anticorrelation of volcanism and glaciation in California over the past 800,000 years. *Geophys. Res. Lett.* (1999). doi:10.1029/1999GL900333

16. Bindeman, I. N. & Lowenstern, J. B. Low-δD hydration rinds in Yellowstone perlites record rapid syneruptive hydration during glacial and interglacial conditions. *Contrib. to Mineral. Petrol.* **171**, 1–24 (2016).

17. Richmond, G. M. Stratigraphy and chronology of glaciations in Yellowstone National Park. *Quat. Sci. Rev.* (1986). doi:10.1016/0277-3791(86)90177-0

18. Huang, H. H. *et al.* The Yellowstone magmatic system from the mantle plume to the

upper crust. *Science (80-.).* (2015). doi:10.1126/science.aaa5648

19. Werner, C. & Brantley, S. CO2 emissions from the Yellowstone volcanic system. *Geochemistry, Geophys. Geosystems* (2003). doi:10.1029/2002GC000473

20. Rose, I., Buffett, B. & Heister, T. Stability and accuracy of free surface time integration in viscous flows. *Phys. Earth Planet. Inter.* (2017). doi:10.1016/j.pepi.2016.11.007

21. Kronbichler, M., Heister, T. & Bangerth, W. High accuracy mantle convection simulation through modern numerical methods. *Geophys. J. Int.* (2012). doi:10.1111/j.1365-246X.2012.05609.x

22. Shaw, D. M. Continuous (dynamic) melting theory revisited. *Can. Mineral.* **38**, 1041–1063 (2000).

23. Slater, L., Jull, M., McKenzie, D. & Gronvöld, K. Deglaciation effects on mantle melting under Iceland: Results from the northern volcanic zone. *Earth Planet. Sci. Lett.* (1998). doi:10.1016/S0012-821X(98)00200-3

24. Barry, P. H., Hilton, D. R., Füri, E., Halldórsson, S. A. & Grönvold, K. Carbon isotope and abundance systematics of Icelandic geothermal gases, fluids and subglacial basalts with implications for mantle plume-related CO2 fluxes. *Geochim. Cosmochim. Acta* (2014). doi:10.1016/j.gca.2014.02.038

25. Armitage, J. J., Ferguson, D. J., Petersen, K. D. & Creyts, T. T. The Importance of Icelandic Ice Sheet Growth and Retreat on Mantle CO2 Flux. *Geophys. Res. Lett.* (2019). doi:10.1029/2019GL081955

26. Flóvenz, Ó. G. & Saemundsson, K. Heat flow and geothermal processes in Iceland. *Tectonophysics* (1993). doi:10.1016/0040-1951(93)90253-G

27. Deines, P. The carbon isotope geochemistry of mantle xenoliths. *Earth-Science Rev.* (2002). doi:10.1016/S0012-8252(02)00064-8

28. Hurwitz, S., Harris, R. N., Werner, C. A. & Murphy, F. Heat flow in vapor dominated areas of the Yellowstone Plateau Volcanic Field: Implications for the thermal budget of the Yellowstone Caldera. *J. Geophys. Res. Solid Earth* (2012). doi:10.1029/2012JB009463

29. Hildreth, W., Halliday, A. N. & Christiansen, R. L. Isotopic and chemical evidence concerning the genesis and contamination of basaltic and rhyolitic magma beneath the yellowstone plateau volcanic field. *J. Petrol.* **32**, 63–138 (1991).

30. Bennett, K. M. Petrogenesis of Pleistocene basalts in the Norris-Mammoth Corridor , Yellowstone National Park. 131 (2006).

31. Wilson, A. M. & Russell, J. K. Glacial pumping of a magma-charged lithosphere: A model for glaciovolcanic causality in magmatic arcs. *Earth Planet. Sci. Lett.* (2020). doi:10.1016/j.epsl.2020.116500

32. Stelten, M. E., Cooper, K. M., Wimpenny, J. B., Vazquez, J. A. & Yin, Q. Z. The role of mantle-derived magmas in the isotopic evolution of Yellowstone's magmatic system. *Geochemistry, Geophys. Geosystems* (2017). doi:10.1002/2016GC006664

33. Tulaczyk, S., Kamb, W. B. & Engelhardt, H. F. Basal mechanics of Ice Stream B, west

Antarctica: 2. Undrained plastic bed model. *J. Geophys. Res. Solid Earth* **105**, 483–494 (2000).

34. Annen, C. & Sparks, R. S. J. Effects of repetitive emplacement of basaltic intrusions on thermal evolution and melt generation in the crust. *Earth Planet. Sci. Lett.* (2002). doi:10.1016/S0012-821X(02)00929-9

35. Patton, H., Hubbard, A., Bradwell, T. & Schomacker, A. The configuration, sensitivity and rapid retreat of the Late Weichselian Icelandic ice sheet. *Earth-Science Reviews* (2017). doi:10.1016/j.earscirev.2017.02.001

36. Bourgeois, O., Dauteuil, O. & Van Vliet-Lanoë, B. Geothermal control on flow patterns in the last glacial maximum ice sheet of Iceland. *Earth Surf. Process. Landforms* (2000). doi:10.1002/(SICI)1096-9837(200001)25:1<59::AID-ESP48>3.0.CO;2-T

37. Fournier, R. O. & Pitt, A. M. The Yellowstone magmatic-hydrothermal system, U.S.A. in *1985 International Symposium on Geothermal Energy: International Volume* 319–327 (1985).

38. Lowenstern, J. B. Carbon dioxide in magmas and implications for hydrothermal systems. *Miner. Depos.* (2001). doi:10.1007/s001260100185

39. Muffler, L. J. P., White, D. E. & Truesdell, A. H. Hydrothermal explosion craters in Yellowstone National Park. *Bull. Geol. Soc. Am.* (1971). doi:10.1130/0016-7606(1971)82[723:HECIYN]2.0.CO;2

40. Hampel, A., Hetzel, R. & Densmore, A. L. Postglacial slip-rate increase on the Teton

normal fault, northern Basin and Range Province, caused by melting of the Yellowstone ice cap and deglaciation of the Teton Range? *Geology* **35**, 1107–1110 (2007).

41. De Vries, M. V. W., Bingham, R. G. & Hein, A. S. A new volcanic province: An inventory of subglacial volcanoes in West Antarctica. in *Geological Society Special Publication* (2018). doi:10.1144/SP461.7

42. An, M. *et al.* Temperature, lithosphere-asthenosphere boundary, and heat flux beneath the Antarctic Plate inferred from seismic velocities. *J. Geophys. Res. Solid Earth* (2015). doi:10.1002/2015JB011917

43. Behrendt, J. C., LeMasurier, W. E. & Cooper, A. K. The West Antarctic Rift System—A Propagating Rift 'Captured' by a Mantle Plume? in *Recent Progress in Antarctic Earth Science* (1992).

44. Scherer, R. P. *et al.* Pleistocene Collapse of the West Antarctic Ice Sheet. *Science (80-.).* **281**, 82–85 (1998).

45. Pollard, D. & DeConto, R. M. Modelling West Antarctic ice sheet growth and collapse through the past five million years. *Nature* (2009). doi:10.1038/nature07809

46. Giacomoni, P. P. *et al.* Long-term storage of subduction-related volatiles in Northern Victoria Land lithospheric mantle: Insight from olivine-hosted melt inclusions from McMurdo basic lavas (Antarctica). *Lithos* (2020). doi:10.1016/j.lithos.2020.105826

47. Hirth, G. & Kohlstedt, D. Rheology of the upper mantle and the mantle wedge: A view from the experimentalists. in *Geophysical Monograph Series* (2003).

doi:10.1029/138GM06

48. Ito, G., Lin, J. & Gable, C. W. Dynamics of mantle flow and melting at a ridge-centered hotspot: Iceland and the Mid-Atlantic Ridge. *Earth Planet. Sci. Lett.* (1996). doi:10.1016/0012-821x(96)00151-3

49. Smith, R. B. *et al.* Geodynamics of the Yellowstone hotspot and mantle plume: Seismic and GPS imaging, kinematics, and mantle flow. *J. Volcanol. Geotherm. Res.* (2009). doi:10.1016/j.jvolgeores.2009.08.020

50. Steinberger, B. Plumes in a convecting mantle ’ Models and observations for individual hotspots depth has usually been assumed Yellowstone show under southern Africa and the south central Hotspot surface but sometimes fixed hotspots give the best fit . In some cases wher. *J. Geophys. Res.* **105**, (2000).

51. Eksinchol, I., Rudge, J. F. & Maclennan, J. Rate of Melt Ascent Beneath Iceland From the Magmatic Response to Deglaciation. *Geochemistry, Geophys. Geosystems* (2019). doi:10.1029/2019GC008222

52. Dannberg, J. & Heister, T. Compressible magma/mantle dynamics: 3-D, adaptive simulations in ASPECT. *Geophys. J. Int.* (2016). doi:10.1093/gji/ggw329

53. Katz, R. F., Spiegelman, M. & Langmuir, C. H. A new parameterization of hydrous mantle melting. *Geochemistry, Geophys. Geosystems* (2003). doi:10.1029/2002GC000433

54. Darbyshire, F. A., White, R. S. & Priestley, K. F. Structure of the crust and uppermost mantle of Iceland from a combined seismic and gravity study. *Earth Planet. Sci. Lett.*

(2000). doi:10.1016/S0012-821X(00)00206-5

55. White, R. S., Minshull, T. A., Bickle, M. J. & Robinson, C. J. Melt generation at very slow-spreading oceanic ridges: Constraints from geochemical and geophysical data. *J. Petrol.* **42**, 1171–1196 (2001).

56. Schutt, D. L., Dueker, K. & Yuan, H. Crust and upper mantle velocity structure of the Yellowstone hot spot and surroundings. *J. Geophys. Res. Solid Earth* **113**, 1–14 (2008).

57. Leeman, W. P., Schutt, D. L. & Hughes, S. S. Thermal structure beneath the Snake River Plain: Implications for the Yellowstone hotspot. *J. Volcanol. Geotherm. Res.* (2009). doi:10.1016/j.jvolgeores.2009.01.034

58. McMillan, N., Larson, P., Fairley, J., Mulvaney-Norris, J. & Lindsey, C. Direct measurement of advective heat flux from several Yellowstone hot springs, Wyoming, USA. *Geosphere* (2018). doi:10.1130/GES01598.1

59. Hurwitz, S. & Lowenstern, J. B. Dynamics of the Yellowstone hydrothermal system. *Reviews of Geophysics* (2014). doi:10.1002/2014RG000452

60. Kelemen, P. B., Yogodzinski, G. M. & Scholl, D. W. Along-strike variation in the aleutian island arc: Genesis of high Mg# andesite and implications for continental crust. in *Geophysical Monograph Series* **138**, 223–276 (2003).

61. Rosenthal, A., Hauri, E. H. & Hirschmann, M. M. Experimental determination of C, F, and H partitioning between mantle minerals and carbonated basalt, CO2/Ba and CO2/Nb systematics of partial melting, and the CO2contents of basaltic source regions. *Earth*

Planet. Sci. Lett. **412**, 77–87 (2015).

62. Miller, W. G. R. *et al.* Estimating the carbon content of the deep mantle with Icelandic melt inclusions. *Earth Planet. Sci. Lett.* (2019). doi:10.1016/j.epsl.2019.07.002

63. Hauri, E. H. *et al.* CO2 content beneath northern Iceland and the variability of mantle carbon. *Geology* (2018). doi:10.1130/G39413.1

64. Pan, V., Holloway, J. R. & Hervig, R. L. The pressure and temperature dependence of carbon dioxide solubility in tholeiitic basalt melts. *Geochim. Cosmochim. Acta* (1991). doi:10.1016/0016-7037(91)90130-W

65. Bohrson, W. A. & Spera, F. J. Energy-constrained open-system magmatic processes II: Application of energy- constrained assimilation - Fractional crystallization (EC-AFC) model to magmatic systems. *J. Petrol.* (2001). doi:10.1093/petrology/42.5.1019

66. Christiansen, R. L., Foulger, G. R. & Evans, J. R. Upper-mantle origin of the Yellowstone hotspot. *Bull. Geol. Soc. Am.* (2002). doi:10.1130/0016-7606(2002)114<1245:UMOOTY>2.0.CO;2

67. Sun, S. -s. & McDonough, W. F. Chemical and isotopic systematics of oceanic basalts: implications for mantle composition and processes. *Geol. Soc. London, Spec. Publ.* **42**, 313–345 (1989).

Supplemental Information

S1. Benchmark against Jull and McKenzie

We benchmark our numerical model against the semi-analytical model of melt production beneath Iceland of Jull and McKenzie[1], hereafter JM96. Specifically, we replicate their constant mantle potential temperature model, using the same parameters – a viscoelastic half-space of viscosity 8×10^{18} Pa s and shear modulus 0.25×10^{11} Pa, and a parabolic ice sheet extending 180 km in radius and 2 km thick, thinning uniformly over 1000 years.

We reproduce rates of pressure change that are similar in magnitude (compare our Figure S1 with Figure 3 of JM96, noting different x-axes). During unloading (t = 10–9 ka in JM96; first two panels in Figure S1) the contours of pressure change follow the same pattern. The depth of maximum pressure change after unloading ($t < 9$ ka; bottom panel) is shallower in our model. This may be attributed to the Cartesian load implied by our 2-D model, whereas JM96 employ a radially-symmetric load.

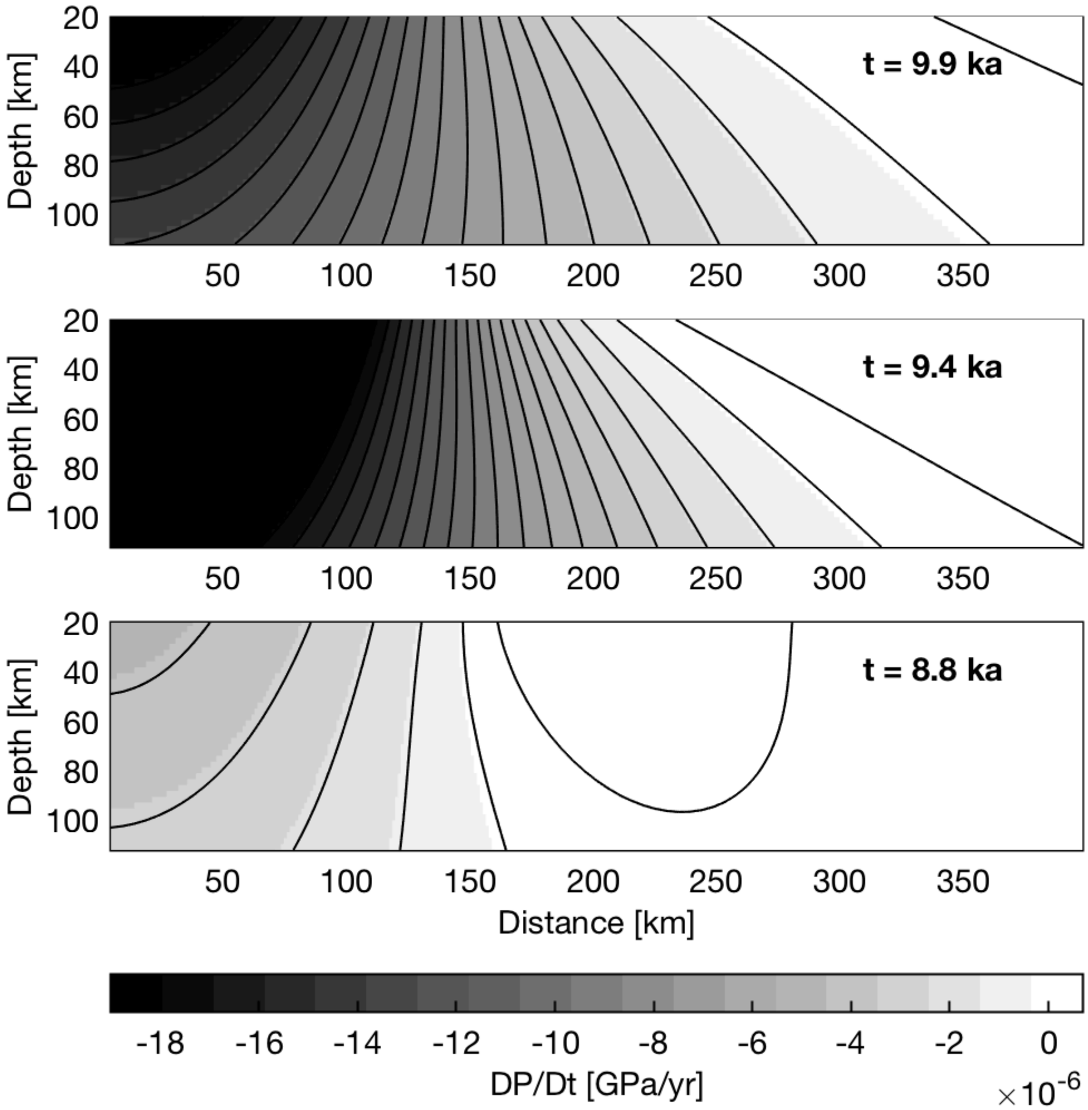

Figure S1: Rates of pressure change, *at different time steps during unloading (10–9 ka). Comparable with figure 3 of JM96.*

We then calculate the total melt production rate (Figure S2). Our 2-D model and melt production rate should be equivalent to the values they obtain at the ridge axis, at the x-intercept of their Figure 10a (red stars, Figure S2). JM96 do not specify which solidus they use, but they do limit the region of melting using a 45° triangle truncated at depths 20-112 km. We obtain similar results with the dry solidus of Katz et al.[53], limited over the same region (compare red lines and stars in Figure S2).

We examine step-by-step the different assumptions made in the JM96 model and our primary model, to explain why our estimate is more productive. The main difference arises from the inclusion of enhanced melting from the wings of the melting region in our model (compare red and dashed blue lines in Figure S2). JM96 had limited the width of the triangle to 92 km. It is unclear whether (and how rapidly) these peripheral melts would be focused to the ridge axis. The inclusion of the temperature derivative in calculating the rate of melt fraction change lessens melt production considerably (compare dashed and solid blue lines). Finally, the dynamically-consistent plume thermal structure (compare green and blue line) and the inclusion of thermal buoyancy (compare black and green line) also increase melt production.

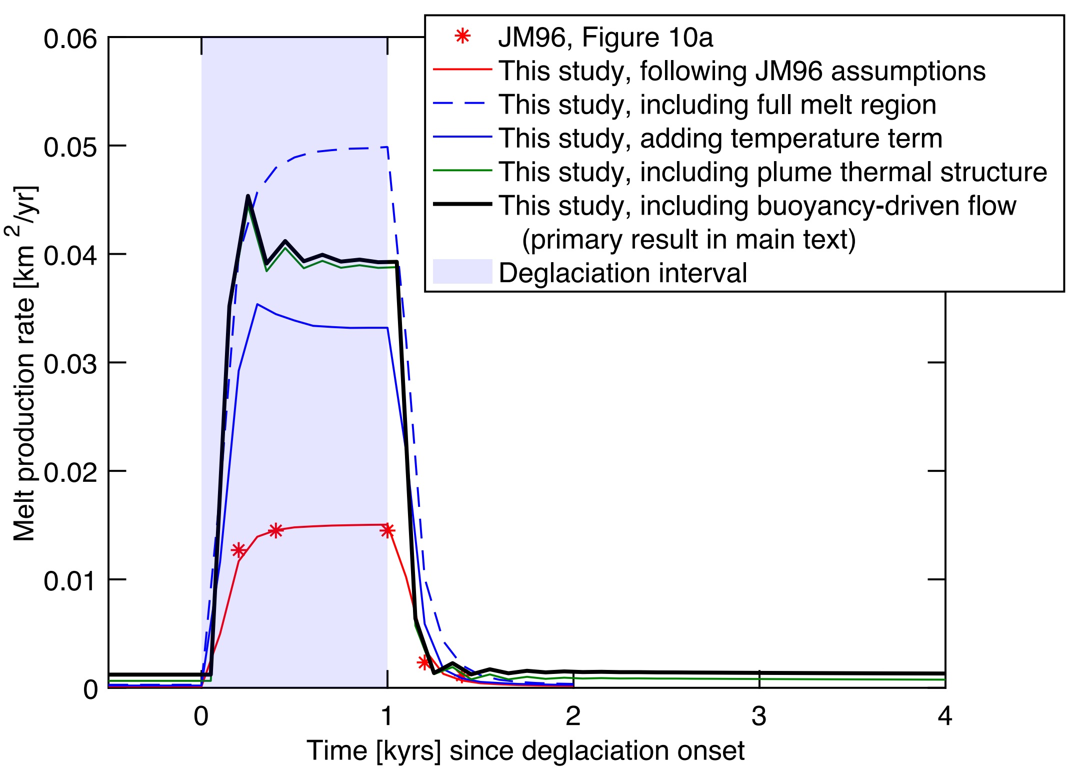

Figure S2: Model runs illustrating step-by-step the effect of modifying assumptions from JM96 *(all under the same glacial forcing). Their results are plotted as red stars. The red line is the most similar/benchmark run, in which the melting region is limited to a truncated triangle extending 92 km off-axis. The dashed blue line shows the effect of using the full melt region predicted by the Katz et al.*[53] *solidus. The solid blue line shows the effect of including the dependence of melting rate on temperature changes. The green line shows the effect of using the plume thermal structure, but turning thermal buoyancy off. The thick black line shows the dynamically-consistent model with the plume thermal structure and buoyancy-driven flow, as presented in main text.*

Finally, we calculate trace element profiles using the melt fractions and melt production rates from the JM96 benchmark. Despite using a different method and partition coefficients, we approximate their reported 15% depletion for the LREE and near 0% for the HREE (Figure S3), when comparing unloading timesteps to background timesteps. While assuming a larger retained melt fraction of 3 wt.% yields the best agreement with JM96 (dashed red line, Figure S3), a smaller value of 1 wt.% (solid lines, Figure S3) better matches observations and is used in the remainder of this study. A comparison of our JM96 benchmark (solid red line) against that of our primary model presented in the main text (solid black line) yields larger depletion of trace elements (~60 %). This may be attributed to the vertical retreat of the ice sheet margins, over a wider melting region.

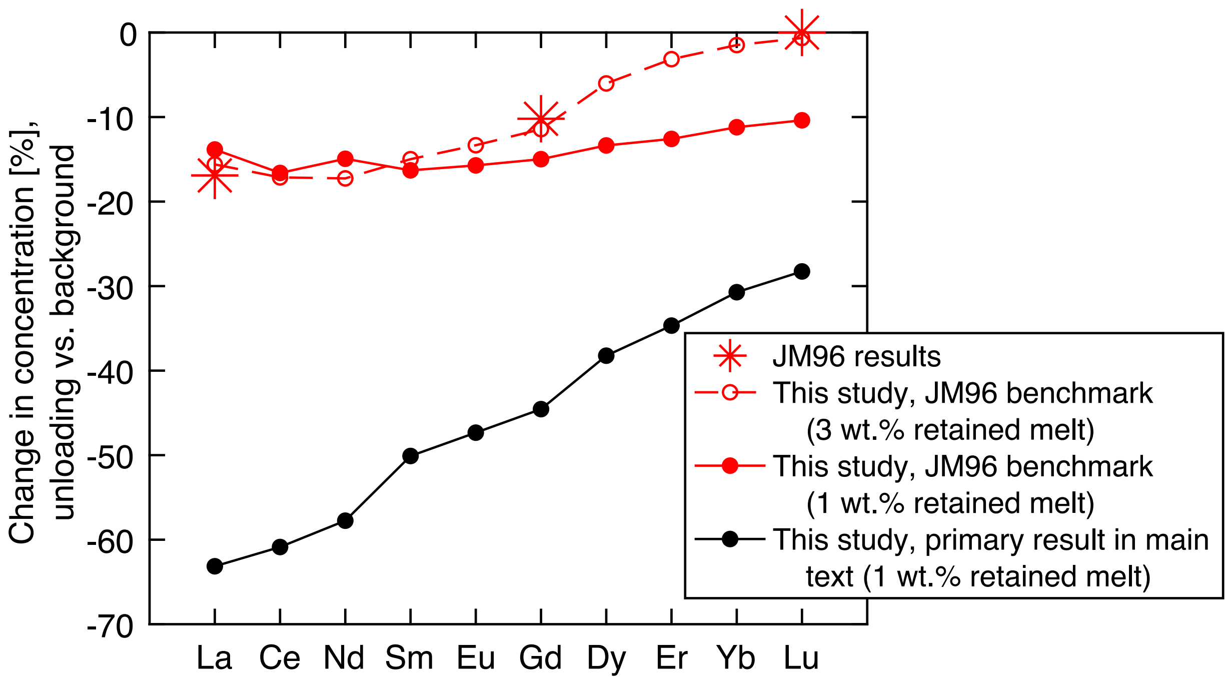

Figure S3: Percent change in trace element concentrations*, for an unloading time step (halfway through deglaciation) relative to the background. Our results for the benchmark model (red lines) agree with that of JM96 (red stars). Our results for the primary model (black line) presented in the main text and Figure S9a predict a more important change.*

S2. Iceland

S2.1 Effect of ice sheet history

We model the effect of the different loading functions used by JM96 (thinning parabola), Eksinchol et al.[51] (viscous gravity current), and this study (retreating parabola). For the models in which the ice sheet retreats inwards, high rates of decompression are initially localized off-axis and then move inwards to the ridge axis. As the mantle is most productive at the axis, the horizontal retreat models predict an increase in total melt production rate through time, while the thinning model from JM96 stays relatively constant during the deglaciation interval (Figure S4a).

The viscous gravity current function involves smaller ice volumes, leading to lower melt production rates (green, Figure S4). The total volume of melt produced over the entire deglacial interval scales with the volume of ice lost.

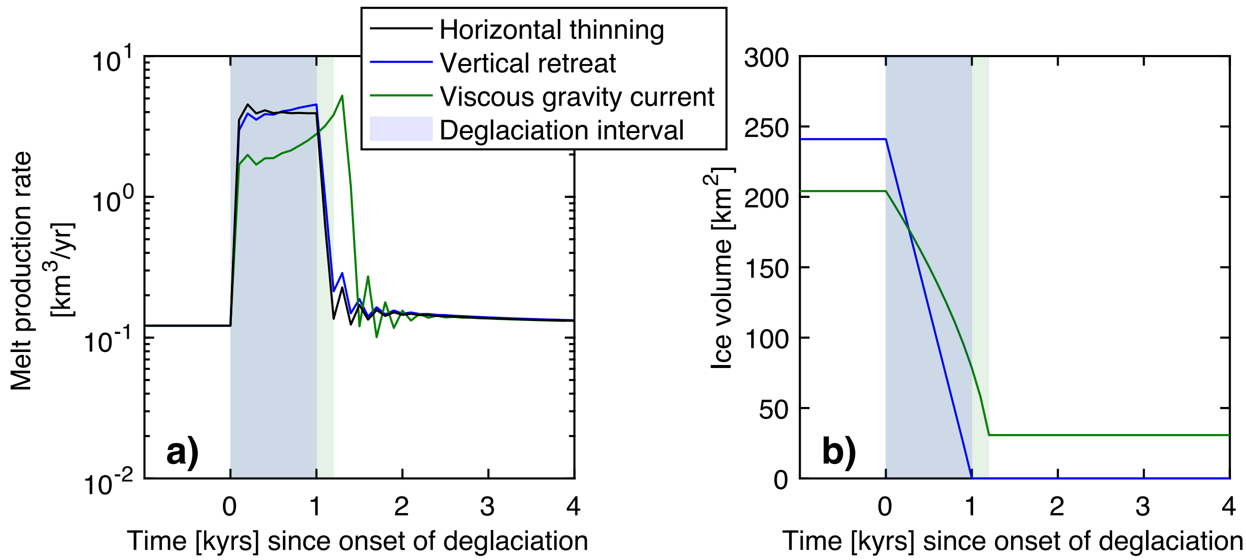

Figure S4: Effect of different loading functions on melt production rate *(a), including a horizontally thinning parabola as in JM96 (black), a parabola retreating vertically from margins as in main text (blue), and a viscous gravity current (from ref.* [51]*). Corresponding ice volumes in 2-D are plotted in b).*

S2.2 Effect of spreading rate and mantle temperature

The primary model run presented in the main text of this study (blue line in Figure S5) has a spreading rate of 10 mm/yr and a mantle potential temperature of 1300 °C, excluding the excess plume temperature of 175 °C. In the absence of a plume, these parameters yield a steady-state crustal thickness of 7 km. Faster spreading rates of 20 mm/yr (purple line) and warmer mantle temperatures of 1320°C (red line) increase rates of melting prior to and during glacial unloading.

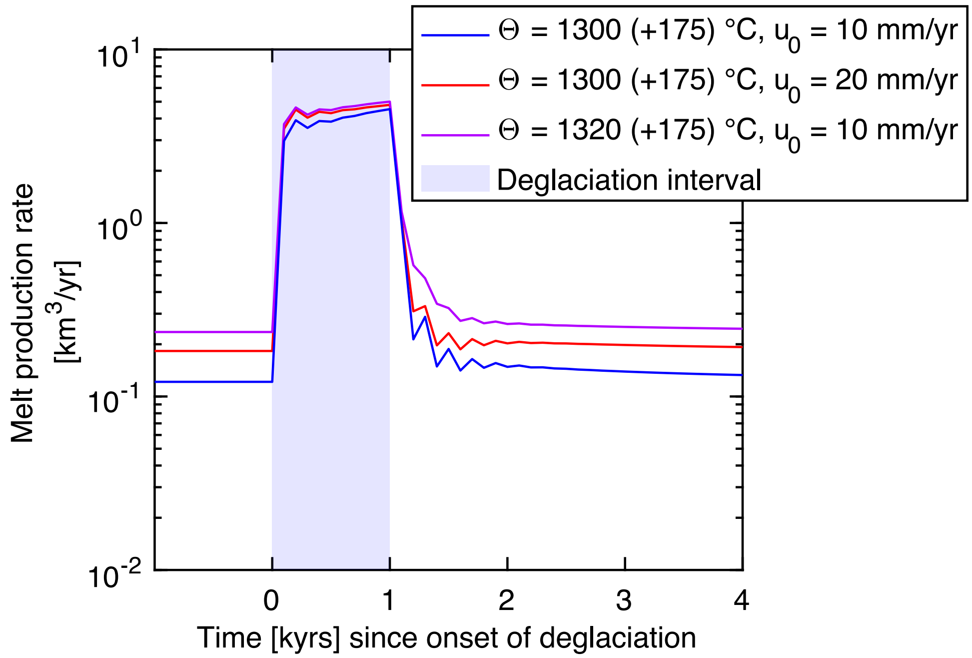

Figure S5: Effect of increasing temperature and spreading rate. *Melt production rates for the case presented in the main text (blue), for a doubled spreading rate (red), and for a raised mantle potential temperature (purple).*

S3 Yellowstone

S3.1 Effect of mantle temperature

The primary model for Yellowstone presented in the main text has a background mantle potential temperature 1320°C, plus an excess plume temperature of 80°C (i.e. 1400°C mantle potential temperature at the plume center). These parameters yield a background mantle melt production rate of 0.022 km^3/yr (black lines in Figures S6a and 3c), within the range of estimated crustal emplacement rates of basaltic mantle melts[19,29]. We explore the effect of increasing the background mantle temperature to 1340°C and 1380°C, yielding background mantle melt production rates of 0.05 km^3/yr (as in ref. [58]) and 0.3 km^3/yr (as in ref. [59]), respectively. To calculate CO_2 fluxes (Figures S6b and 3e), we use mantle source CO_2 concentrations of 300–500 ppm in the 1320°C case, 280–460 ppm in the 1340°C case, and 25–37 ppm in the 1380°C case. These concentrations yield background CO_2 fluxes of 6.0–10.1 Mt/yr, consistent with modern constraints[19].

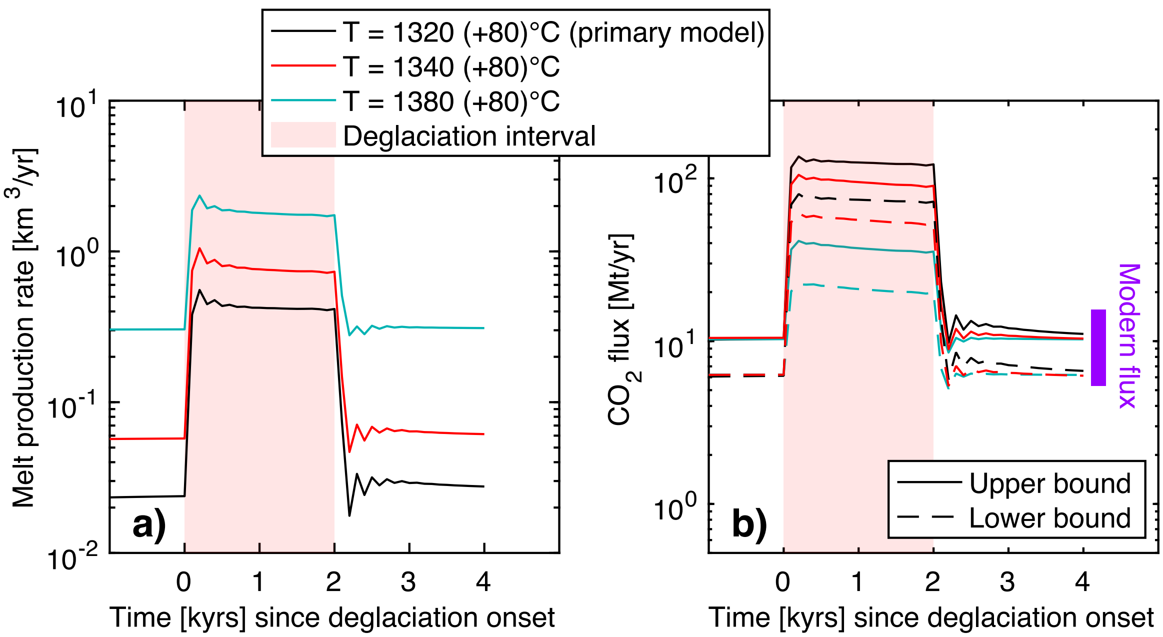

Figure S6: Effect of higher mantle temperatures, *on melt production rates a) and CO_2 flux b). Black lines are results presented in the main text. Source mantle CO_2 concentrations in b) are varied to match the modern flux (purple bars).*

S3.2 Yellowstone without plume

While it is established that there is additional melting in the upper mantle beneath Yellowstone, the presence of a mantle plume extending to depths of 600 km or greater remains controversial[66]. We perform a run in which we remove the plume tail, to understand its effect on our model. To do so, we artificially lower the temperature of the mantle at greater depths (>150 km), such that only an upper mantle thermal anomaly remains. Removing the plume tail and reducing the influx of material lessens upwelling from the lower mantle. We find the rates of pressure change in the melting region during unloading are similar, implying the presence/absence of the plume tail itself does not affect our results (they are instead controlled primarily by the viscosity of the upper mantle in the melting region, and overlying lithosphere). As the thermal anomaly at the base of the lithosphere was originally set by the plume, this test is not equivalent to explicitly modeling another mechanism (e.g., edge-driven subduction from the slab).

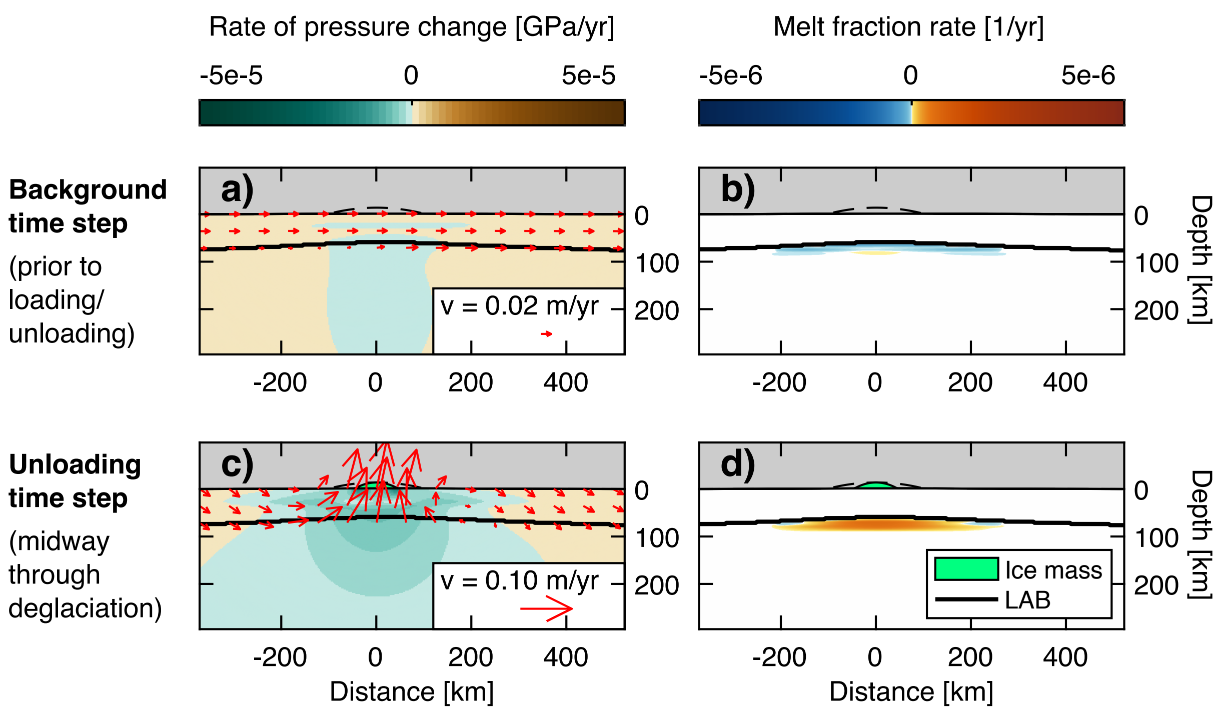

***Figure S7**: In the absence of a plume, effect of deglaciation of Yellowstone ice cap* *(green parabola) on rates of pressure change (a,c, teal-brown colors) and rates of melt fraction change (b,d, blue-orange colors). The top row shows a model time step prior to any glacial* *loading/unloading, while the bottom row shows a time step halfway through the deglaciation (1000 years following its onset). Red arrows show mantle flow, the thick black line is the LAB (T=1300℃).*

S3.3 Effect of loading function

Given the thickness of the lithosphere and the great depth of melting beneath Yellowstone, the pressure changes due to unloading are distributed throughout the melting zone. As a result, the style of the ice cap retreat is unimportant (Figure S8a). Ice caps which are thinned horizontally yield nearly identical rates of melt production as ice caps which retreat vertically, upon radial integration. If the ice cap retreats more slowly, the melt production rate decreases proportionately but the total volume of extra melt produced is unchanged. Our estimates of the total extra melt and CO_2 are produced by the end of the deglaciation does not depend on the manner in which the ice cap retreats, given a constant initial ice volume.

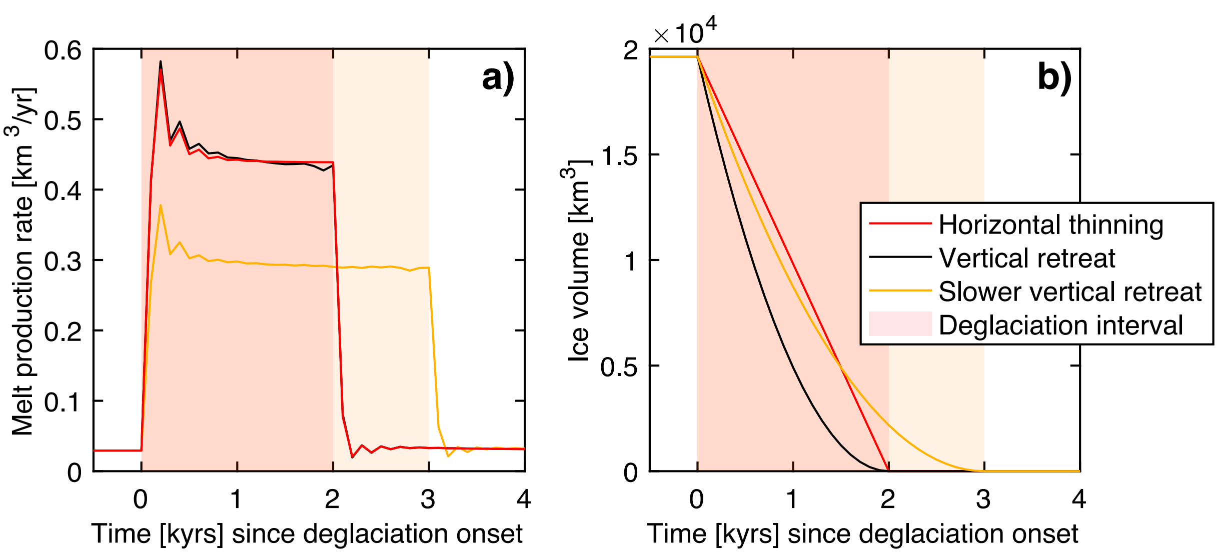

***Figure S8: Effect of different loading functions on melt production rate** (a), including a horizontally thinning parabola (red), a parabola retreating vertically from margins as in main text (black), and a slower deglaciation lasting 3000 years (orange). Corresponding radially-integrated ice volumes are plotted in b).*

S4. Trace elements

We calculate trace element profiles for both Iceland and Yellowstone (Figure S9). These profiles compare well with erupted basalts, which provides support for the CO_2 calculations in the main text. Our modeled Iceland profiles produce a sufficiently large percent change between background and unloading time step (Figure S9a). For Yellowstone, trace element compositions both before and during unloading are within the range of the data (Figure S9b). None of these basalts were dated to the Bull Lake deglaciation (140-150 ka). The percent change predicted by the model (~30%) may be too small to be detected, even if basalts dated to the deglaciation were found.

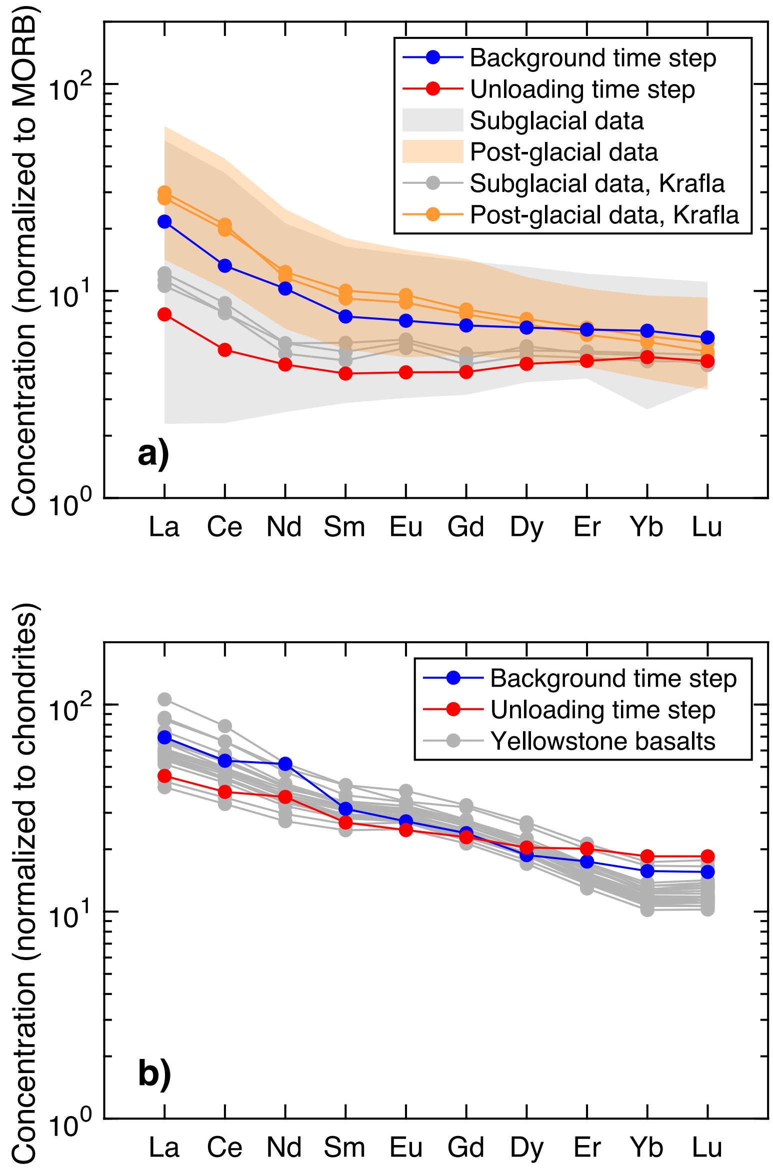

Figure S9: Trace element concentrations before and during unloading. *a) Iceland model results compared to data from Maclennan et al.*[5] *b) Yellowstone model results compared to data from Bennett*[30]*. The Iceland and Yellowstone data are normalized to MORB and chondrites, respectively (using ref.* [67]*), for ease of comparison with the original datasets.*